Development and validation of a nonlinear dynamic model for tuned liquid multiple columns dampers

Liang Cao[a,*], Yongqiang Gong[b], Filippo Ubertini[c], Hao Wu[b], An Chen[b], Simon Laflamme[b,d]

[a] *ATLSS Engineering Research Center, Lehigh University, Bethlehem, PA 18015, U.S.A*
[b] *Department of Civil, Construction, and Environmental Engineering, Iowa State University, Ames, IA 50011, U.S.A*
[c] *Department of Civil and Environmental Engineering, University of Perugia, Perugia, Italy*
[d] *Department of Electrical and Computer Engineering, Iowa State University, Ames, IA 50011, U.S.A*

Abstract

The tuned liquid column damper (TLCD), a passive damping device consisting of a large U-tube with oscillating liquid, has been shown to be effective at mitigating structural responses under natural hazards. Aside from their bandwidth-limited mitigation capabilities, a key limitation of TLCDs is in their large geometries that occupy large space often at prime locations. A solution is to implement multi-columned versions, termed tuned liquid multiple columns dampers (TLMCDs), which have the potential to be tuned to multiple frequencies and occupy less space by leveraging the multiple columns to allow fluid movement. However, mathematical models characterizing their dynamic behavior must be developed enabling proper tuning and sizing in the design process. In this paper, a new analytical model characterizing a TLMCD as a multiple degrees-of-freedom coupled nonlinear system is presented. The frequencies of free vibration and vibration modes of a TLMCD are identified in closed-form formulations. Results are validated using computational fluid dynamics simulations, and show that the analytical model can predict the damper's liquid surface movements as well as its capability to reduce structural vibration when the structure is subjected to harmonic excitations. A parametric study is conducted to investigate the effect of head loss coefficients, column spacing, cross-section area ratios, and column numbers on mitigating structural response. It is found that, while TLMCDs are less effective than traditional TLCDs under an equal liquid mass, they can provide enhanced performance under geometric restrictions.

Keywords:
Tuned liquid column damper, structural control, damping, passive control, analytical solution, computational fluid dynamics

1. Introduction

Advances in construction methods and materials have led to more flexible structures, thereby raising the demand on reducing vibrations caused by natural hazards. Such vibrations can be mitigated through the incorporation of supplemental damping devices, including passive [1, 2], semi-active [3, 4, 5] and active [6, 7]

*Corresponding author
Email address: lic418@lehigh.edu (Liang Cao)

systems. Of interest to this paper are passive systems, which have been widely accepted by the field due to their mechanical robustness and mitigation performance without necessitating external power [8]. Amongst these are tuned mass dampers (TMDs), which dissipate energy by leveraging inertia. TMDs are typically effective at +/- 15% of their tuned frequency, making them ideal at mitigating wind-induced vibrations [9]. A variation of TMDs is the tuned liquid column damper (TLCD), which consists of a large U-shaped tube with oscillating liquid. TLCDs leverage gravity in the vertical tubes as the restoring forces and generate damping from the liquid head loss induced by an internal orifice located in the horizontal section of the U-shaped tube. TLCDs have low installation and maintenance costs, high mechanical robustness, and can be used for storage of water [10].

In TLCD modeling, liquid surface displacements are frequently used to represent liquid motion in vertical columns, because the column cross-section sizes are relatively small compared to their lengths. In civil engineering applications, liquid compression is often negligible and ignored, whereby a TLCD with two free liquid surfaces can be modeld as a single degree-of-freedom (SDOF) system. Sakai *et al.* [11] analytically modeled the liquid motion of a TLCD using a weakly nonlinear equation with nonlinear damping provided by the internal orifice in the horizontal column. Others have studied numerical solutions for TLCD-structure interactions [12, 13]. Transfer functions have also been applied to predict the frequency response of an undamped SDOF structure equipped with a TLCD under harmonic or white noise excitations, assuming that the nonlinear damping term in the TLCD equation can be replaced with an equivalent linear one [14, 15, 16].

Analogous to TMDs, TLCDs are only effective in a restricted fixed frequency range. Variations of TLCDs have been proposed in the last few decades to address such limitation. One example is the bidirectional TLCD, first proposed by Hitchcock [17] and further developed by Razos *et al.* [18]. Bidirectional TLCDs consist of four vertical columns and work as two TLCDs installed orthogonally, useful at mitigating vibrations from orthogonal directions. Min *et al.* [19] proposed a multi-cell re-tuning passive TLCD, in which the two vertical columns are subdivided into a number of smaller cells that can be sealed or opened to adjust the damper's frequency of free vibration after installation. Recently, the authors introduced the concept of tuned liquid wall damper (TLWD) [20], which is a small multi-capillary TLCD encased in concrete walls. The TLWD is designed to use the liquid for both thermal storage and structural damping. The TLWD is also a multi-cell TLCD. This type of TLCD system is here termed tuned liquid multiple columns dampers (TLMCDs). The critical advantage of TLMCDs is in their capability to be tuned at multiple frequencies, and availability of multiple columns yielding smaller overall geometries. The development of mathematical models characterizing their dynamic behavior could greatly facilitate their holistic integration within the structural design phase via a motion-based design procedure.

The extension of TLCD models to TLMCDs is challenging due to the TLMCD's nonlinear equations of motion. Rozas *et al.* [18] modeled bidirectional TLCDs through the assumption that both DOFs in the orthogonal directions were uncoupled. Min *et al.* [19] and Wu *et al.* [20] modeled TLMCDs by transforming

the TLMCD into an equivalent TLCD of the same frequency of free vibration. However, this approximation method introduces unnecessary constraints on the liquid motion by presuming a relationship between liquid surface displacements in different columns. All the above proposed dynamic models are derived from TLCD models, and do not accurately characterize the liquid motion coupling between multiple vertical columns in a TLMCD, where the liquid surface displacement in each column should be treated as an individual DOF. A TLMCD model is also fundamentally different from multiple tuned mass dampers (MTMDs) [21] or multiple tuned liquid column dampers (MTLCDs) [22] models, in which each individual damper is tuned to a different frequency of free vibration to enhance robustness against frequency mistuning with the motion of each individual masses being uncoupled. A TLMCD is an MDOF damper and has multiple coupled frequencies of free vibration and mode shapes. To the best knowledge of the authors, the closest work is that of Hirata and Craik [23], who developed a dynamic model describing the free liquid oscillation in a three-armed vertical columns. However, this model only describes the coupled liquid motion in an undamped and unforced system and cannot characterize nonlinear damping and inertia forces found in a TLMCD.

In this paper, the authors propose a new analytical model to characterize a damped and forced TLMCD system that can extend to unlimited DOFs. Unlike previous TLCD dynamic models, where the liquid damping force is only governed by a single head loss coefficient, the proposed method captures essential features of the liquid damping forces by dividing them into two parts. The first one is induced by the friction phenomenon in the liquid motion. The second one is due to the head loss of fluid flowing through the orifices.

In the next section, the proposed dynamic model for a TLMCD is introduced. After, the time series of a 4-column and an 8-column TLMCD's liquid surface displacements calculated from the dynamic model are validated against computational fluid dynamics (CFD) simulation results. Subsequently, a linearization method for TLMCDs is formulated and the modal shapes at resonance described. It is followed by a parametric study of head loss coefficients, column spacing, cross-section area ratio and column number on the structural response reduction conducted numerically. Then, the effectiveness of TLMCDs and TLCDs are compared both under equal liquid mass and geometries.

2. Analytical model

The typical TLMCD consists of a horizontal tube joining multiple vertical columns. Fig. 1 schematizes an N-column TLMCD, where $\ddot{x}_g$ is the acceleration transmitted from the floor, x_i is the vertical liquid surface displacement in the i^{th} column (positive upwards), h is the initial vertical liquid surface height equal in every columns, l_i is the horizontal centre-to-centre distance between the i^{th} and $i+1^{th}$ columns, ψ_i is the i^{th} orifice blocking ratio, A is the columns' cross-section area, ν is the cross-section area ratio of the vertical tubes to the horizontal tube, and Q_o, Q_f, Q_e are the orifice damping force, the friction force between the liquid and column's inner surface, and the liquid inertia force, respectively. Variables Q_o, Q_f, and Q_e are the nonconservative forces in the TLMCD system, which will be discussed later. The analytical model is built upon the following assumptions: 1) all vertical columns are identical; 2) liquid compression and

liquid-air interface diffusion are negligible, resulting in a constant total liquid volume during vibrations; and 3) the cross-section sizes of columns are considerably smaller than the total length of the tube, resulting in a uniform motion of the liquid surface over the cross section in each column. Under these assumptions, the N-column TLMCD can be treated as N-1 DOFs by letting the displacement of the last column be dependent on the other column motions ($x_N = -\sum_{i=1}^{N-1} x_i$).

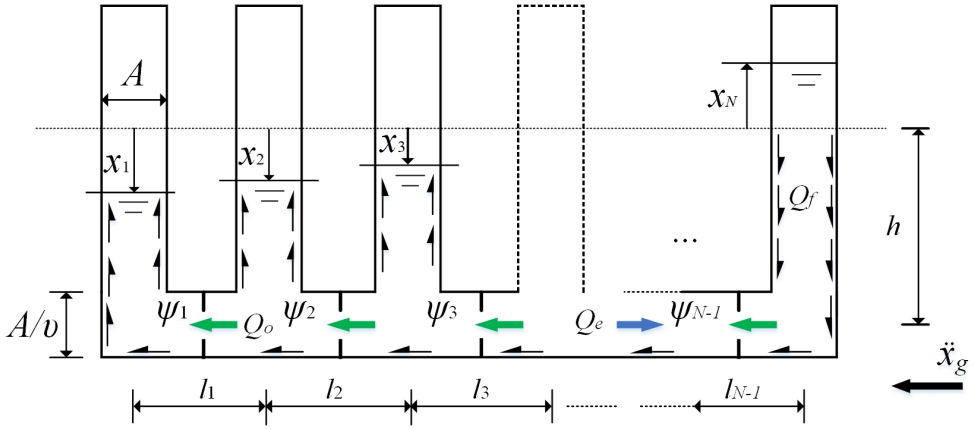

Figure 1: Schematic of an N-column TLMCD (x_i is positive upwards)

The equations of motion for the TLMCD are derived using the Lagrange equations. Similar methods have been adopted by Hitchcock [24], Sarkar *et al.* [25] and Rozas *et al.*[18] for some variants of TLCDs. Starting with

$$\frac{\mathrm{d}}{\mathrm{d}t}\left(\frac{\partial T}{\partial \dot{x}_i}\right) - \frac{\partial T}{\partial x_i} + \frac{\partial V}{\partial x_i} = Q_i, \qquad i = 1, 2, ..., N-1 \tag{1}$$

where $\dot{x}_i$ denotes the liquid velocity in the i^{th} column, t is time, Q_i is the nonconservative force acting on the i^{th} DOF, and T and V are respectively the system's kinematic and potential energy, with

$$V = \frac{1}{2}\rho_l A g \sum_{i=1}^{N} x_i^2 \tag{2a}$$

$$T = \frac{1}{2}\rho_l A \sum_{i=1}^{N} \dot{x}_i^2 (h + x_i) + \frac{1}{2}\rho_l A/\nu \sum_{i=1}^{N-1} \nu^2 l_i \left(\sum_{j=1}^{i} \dot{x}_j\right)^2 \tag{2b}$$

where ρ_l is the liquid density, and g is gravitational acceleration. Using the assumed kinematic constraint $x_N = -\sum_{i=1}^{N-1} x_i$ and substituting Eq. (2) into Eq. (1) gives:

$$\begin{aligned} \sum_{j=1}^{i}\left(\sum_{k=1}^{N-1} x_k - h - \sum_{k=i}^{N-1} \nu l_k\right)\ddot{x}_j + \sum_{j=i+1}^{N-1}\left(\sum_{k=1}^{N-1} x_k - h - \sum_{k=j}^{N-1} \nu l_k\right)\ddot{x}_j - (h + x_i)\ddot{x}_i + \frac{1}{2}\left(\sum_{k=1}^{N-1} \dot{x}_k\right)^2 \\ - \frac{1}{2}\dot{x}_i^2 - g x_i - g\sum_{k=1}^{N-1} x_k + \frac{Q_i}{\rho_l A} = 0, \qquad i = 1, 2, ..., N-1 \end{aligned} \tag{3}$$

The non-conservative force Q_i includes three parts: 1) the damping force Q_{oi} induced by the orifices in the horizontal column; 2) the friction force Q_{fi} between the liquid and column's inner surface; and 3) the liquid inertia force Q_{ei} due to $\ddot{x}_g$.

The damping force Q_{oi} is typically assumed to be proportional to the square of the liquid velocity [12]. The relationship between the head loss coefficient η and orifice blocking ratio ψ has been experimentally studied by Idelchik and Fried [26], Min *et al.*[27], and Wu *et al.* [28]. Idelchik and Fried's formula is selected because it models the effect of the orifices and excludes the friction head loss that is modeled separately in our study

$$\eta = \left(\psi + 0.707\psi^{0.375}\right)^2 (1-\psi)^{-2} \tag{4}$$

It should also be noted that the above empirical equation may not be accurate enough since the head loss coefficient is also influenced by the external excitation's amplitude and type (white noise, harmonic, seismic signal, etc.), and orifice shapes [27, 29]. It is recommended to obtain the relationship experimentally case-by-case. For a small unit of time, work done by the orifice damping force can be written

$$\delta W_o = -\sum_{k=1}^{N-1} \frac{1}{2}\rho_l A \left[\nu\eta_k \left| \sum_{j=1}^{k} \dot{x}_j \right| \left(\sum_{j=1}^{k} \dot{x}_j \right) \sum_{j=1}^{k} \delta x_j \right] \tag{5}$$

where η_k is the head loss coefficient for orifice k. The orifice damping force Q_{oi} acting on each DOF is given by:

$$Q_{oi} = \frac{\partial W_o}{\partial x_i} = -\sum_{k=i}^{N-1} \frac{1}{2}\rho_l A \left[\nu\eta_k \left| \sum_{j=1}^{k} \dot{x}_j \right| \left(\sum_{j=1}^{k} \dot{x}_j \right) \right] \tag{6}$$

For laminar flows, the friction resistance is related to the Reynolds number of the flow and is largely insensitive to surface roughness. However, when the flow is turbulent, the friction force becomes dependent on the roughness of the tube's inner surface. If the liquid in the TLMCD is designed to be contained by coarse pipes, the friction force can be considerably larger than the orifice damping force. For mathematical tractability, we assume that the friction force is proportional to the square of liquid velocity $\dot{x}^2$. An expression for the work done by the friction force over a small unit of time can be obtained:

$$\delta W_f = -\sum_{k=1}^{N} \rho_l A \left[\mu |\dot{x}_k| \dot{x}_k \left(h + x_k\right) \delta x_k\right] + \sum_{k=1}^{N-1} \rho_l A \left[\mu\nu l_k \left| \sum_{j=1}^{k} \dot{x}_j \right| \left(\sum_{j=1}^{k} \dot{x}_j \right) \sum_{j=1}^{k} \delta x_j \right] \tag{7}$$

where μ is the head loss coefficient due to friction. The friction damping force Q_{fi} acting on each DOF is

given by:

$$
\begin{aligned}
Q_{fi} &= \frac{\partial W_f}{\partial x_i} \\
&= -\rho_l A \mu \left\{ |\dot{x}_i| \dot{x}_i \left(h + x_i\right) + \left| \sum_{j=1}^{N-1} \dot{x}_j \right| \left(\sum_{j=1}^{N-1} \dot{x}_j \right) \left(h - \sum_{j=1}^{N-1} x_j \right) + \sum_{k=i}^{N-1} \left[\nu l_k \left| \sum_{j=1}^{k} \dot{x}_j \right| \left(\sum_{j=1}^{k} \dot{x}_j \right) \right] \right\}
\end{aligned} \tag{8}
$$

Other than the orifice blocking flow and the friction force, any other drastic variations in the liquid velocity may result in additional head loss in the damping system. For example, some recent work [30] experimentally found that the transition zone between the vertical columns and the horizontal column is another source of liquid head loss. However, direct formulas for computing this type of head loss are yet to be developed. This effect is not considered in the proposed TLMCD analytical model.

The last non-conservative force is the liquid inertia force Q_{ei} caused by the external acceleration. The work done by the excitation force on the vertical columns is null, because the sum of vertical liquid masses is constant and the direction of inertia forces is perpendicular to the liquid velocity. The work done by the inertia force Q_{ei} is solely from the motion of the liquid in the horizontal column:

$$
\delta W_e = -\rho_l A \sum_{k=1}^{N-1} \left(\ddot{x}_g l_k \sum_{j=1}^{k} \delta x_j \right) \tag{9}
$$

The inertia force Q_{ei} acting on each DOF is:

$$
Q_{ei} = \frac{\partial W_e}{\partial x_i} = -\rho_l A \ddot{x}_g(t) \sum_{k=i}^{N-1} l_k \tag{10}
$$

and the total non-conservative force Q_i acting on the ith degree of freedom is:

$$
Q_i = Q_{oi} + Q_{fi} + Q_{ei} \tag{11}
$$

Combining Eqs.(3), (6), (8), (10), and (11), one obtains the nonlinear equations of motion for a TLMCD:

$$
\begin{aligned}
&\sum_{j=1}^{i} \left(\sum_{k=1}^{N-1} x_k - h - \sum_{k=i}^{N-1} \nu l_k \right) \ddot{x}_j + \sum_{j=i+1}^{N-1} \left(\sum_{k=1}^{N-1} x_k - h - \sum_{k=j}^{N-1} \nu l_k \right) \ddot{x}_j \\
&\qquad - \left(h + x_i\right) \ddot{x}_i + \frac{1}{2} \left(\sum_{k=1}^{N-1} \dot{x}_k \right)^2 - \frac{1}{2} \dot{x}_i^2 - g x_i - g \sum_{k=1}^{N-1} x_k \\
&\qquad = \mu |\dot{x}_i| \dot{x}_i \left(h + x_i\right) + \mu \left| \sum_{k=1}^{N-1} \dot{x}_k \right| \left(\sum_{k=1}^{N-1} \dot{x}_k \right) \left(h - \sum_{k=1}^{N-1} x_k \right) \\
&+ \sum_{k=i}^{N-1} \nu \left(\mu l_k + \frac{1}{2} \eta_k \right) \left| \sum_{j=1}^{k} \dot{x}_j \right| \sum_{j=1}^{k} \dot{x}_j + \ddot{x}_g(t) \sum_{k=i}^{N-1} l_k, \qquad i = 1, 2, ..., N-1
\end{aligned} \tag{12}
$$

which can be written in matrix form

$$\mathbf{M}(\mathbf{x})\ddot{\mathbf{x}} + \mathbf{K}\mathbf{x} + \mathbf{F}(\mathbf{x}, \dot{\mathbf{x}}) = \mathbf{0} \tag{13}$$

where $\mathbf{M}(\mathbf{x}) \in \mathbb{R}^{N-1\times N-1}$ is a state-dependent mass matrix, $\mathbf{K} \in \mathbb{R}^{N-1\times N-1}$ is a linear stiffness matrix, and $\mathbf{F}(\mathbf{x}, \dot{\mathbf{x}}) \in \mathbb{R}^{N-1\times 1}$ is a restoring force matrix containing all the other nonlinear terms. The state-dependent mass matrix $\mathbf{M}(\mathbf{x})$ is given by:

$$\mathbf{M(x)} = \left(\sum_{k=1}^{N-1} x_k - h\right)\mathbf{I} - \begin{bmatrix} x_1 + h + \nu\sum_{k=1}^{N-1} l_k & \nu\sum_{k=2}^{N-1} l_k & \nu\sum_{k=3}^{N-1} l_k & \dots & \nu l_{N-1} \\ \nu\sum_{k=2}^{N-1} l_k & x_2 + h + \nu\sum_{k=2}^{N-1} l_k & \nu\sum_{k=3}^{N-1} l_k & \dots & \nu l_{N-1} \\ \nu\sum_{k=3}^{N-1} l_k & \nu\sum_{k=3}^{N-1} l_k & x_3 + h + \nu\sum_{k=3}^{N-1} l_k & \dots & \nu l_{N-1} \\ \vdots & \vdots & \vdots & \ddots & \vdots \\ \nu l_{N-1} & \nu l_{N-1} & \nu l_{N-1} & \dots & x_{N-1} + h + \nu l_{N-1} \end{bmatrix} \tag{14}$$

where $\mathbf{I}$ is the identity matrix of appropriate size. From Eq. (12), it is noted that the cross-section area A and liquid density ρ_l are not directly related to the liquid motion since they are canceled from both sides of the equation, but they may have an indirect influence on the head loss coefficients. The derivation of a formulation for determining optimal tuning ratios and head loss coefficients for the TLMCD is complex, because the mass matrix is state-dependent.

3. Model validation

In this section, the analytical model is validated against CFD simulations on a 4-column and an 8-column TLMCD, after a brief verification of the CFD methodology itself by comparing results on a TLCD against experimental data reported in literature.

3.1. CFD methodology verification

CFD models are created in ANSYS FLUENT 17.2 software and simulated using a standard k-ε solver, widely used to simulate turbulent flow [31, 32, 33]. The maximum mesh size is set as 0.01 m, with much finer mesh around the orifices in the bottom area. The top of each vertical columns in the TLMCD is open to allow the liquid to flow freely. No liquid and air diffusion is included. To account for the unevenness of the liquid surface in the vertical columns, the liquid surface displacement is defined as the distance between the horizontal centerline of the liquid surface and its original steady state position.

The CFD methodology is first verified against experimental data published in Wu *et al.* [28]. In their study, a TLCD (2-column TLMCD) was directly attached to a shaking table and subjected to a harmonic ground acceleration $\ddot{x}_g = 4\sin(0.492t)$ cm/s^2. The cross-section area of the TLCD tube was reported to be 15 x 15 cm^2, and the horizontal and vertical lengths were 85 cm and 63.75 cm, respectively. The orifice blocking ratio varied from 20% to 80% to obtain a relationship with the TLCD's head loss coefficient. The experimented system without the shaking table was modeled by generating meshes with a maximum element

length of 1 cm to capture features associated with liquid motion in transition areas such as elbows and tee sections. Since the TLCD material is unknown, the roughness height of the pipe was set to 0.002 mm. Results from the CFD simulation are compared against these experimental results in Table 1. Results show slightly lower maximum liquid surface amplitudes, but no more than 10%, showing an overall good agreement between both the experimental and CFD simulation results.

Table 1: Comparison of liquid surface amplitudes (cm) between CFD and test results [28].

orifice blocking ratio ψ	0.2	0.4	0.6	0.8
experimental results	15.8	13.1	9.2	4.3
CFD simulation results	14.3	12.2	8.3	4.3
difference (%)	9.5	7.3	9.7	0

3.2. Validation of analytical model

The proposed analytical model presented in Section 2 is validated on 4-column and 8-column TLMCDs using the same CFD methodology as described in Section 3.1. The geometry parameters and damping coefficients of both systems are listed in Table 2. All the orifices have an identical blocking ratio of 20%, and the orifice head loss coefficient η is determined using Eq. (4). Liquid surface displacements are first calculated using the analytical model and then compared to the CFD results.

Table 2: System parameters for 4-column and 8-column TLMCDs.

system parameters		units	4-column	8-column
cross-section area	A	cm^2	15x15	30x30
orifice head loss coefficient	η	–	0.54	0.54
friction head loss coefficient	μ	–	0.2	0.1
initial liquid surface height	h	m	0.5	0.9
column spacing	l_i	m	0.5	1.5

Two simulation cases are considered: free oscillation and forced vibrations. Starting with the 4-column TLMCD under free oscillation, the initial condition on the liquid surface displacements in the four vertical columns are set to: $x_1(0) = x_2(0) = 0.385$ m, and $x_3(0) = x_4(0) = -0.385$ m. Figs. 2(a) and (b) plot time series data of the four columns' liquid surface displacements from the analytical model and the CFD simulations. There is a good agreement between the model and simulations results. For the forced vibrations case of the 4-column TLMCD, a harmonic base acceleration $\ddot{x}_g = 0.37\sin(2.46t)$ m/s^2 is used as the forcing, where the vibration frequency is at the first frequency of free vibration of the 4-column TLMCD, and the acceleration amplitude is selected arbitrarily to provide a reasonable fluid motion. Fig. 3 shows the liquid motion amplitudes under this harmonic excitation: the liquid heights in the four columns decrease almost

linearly from one end to the other. Fig. 4(a) and (b) are plots of the forced vibration results for the liquid surface displacements for all the columns, also showing a good agreement between the model and simulation results.

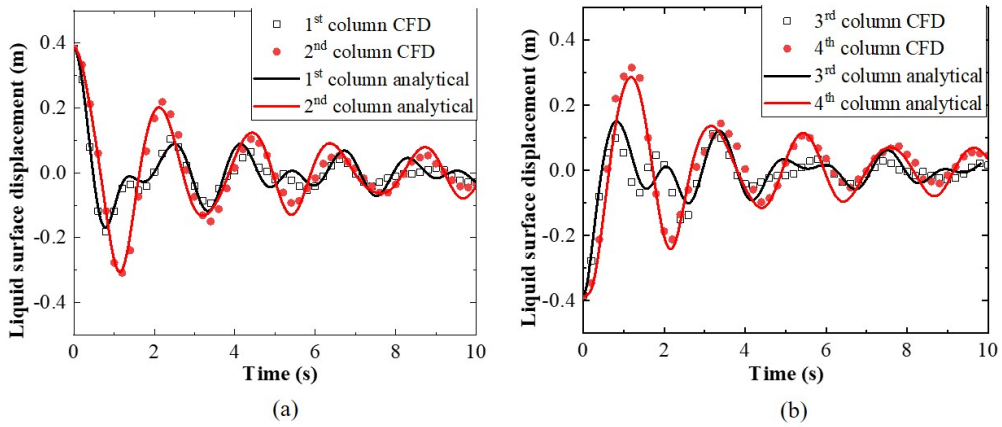

Figure 2: Time series of column displacements under free oscillation: (a) columns x_1 and x_2; and (b) columns x_3 and x_4.

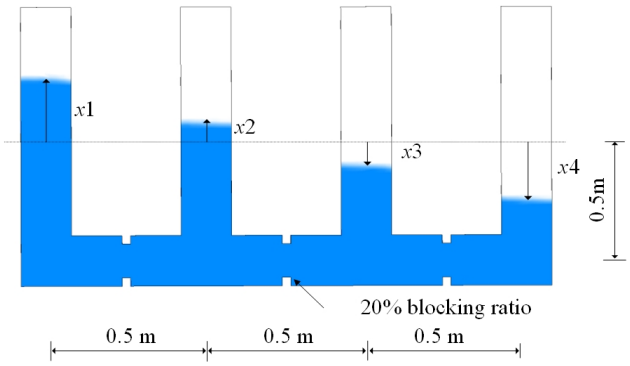

Figure 3: CFD results of the 4-column TLMCD under forced vibration, $t = 7.8$ s.

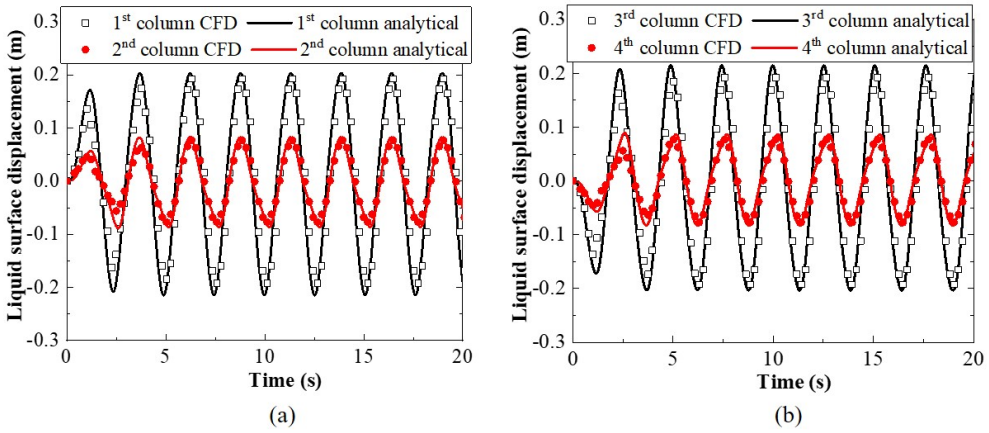

Figure 4: Time series of column displacements under forced oscillation: (a) columns x_1 and x_2; and (b) columns x_3 and x_4.

The 8-column TLMCD is validated using the same methodology as for the 4-column TLCD. Figs. 6 and 7 plot the time series data comparing the results of both free and force vibrations. For the free vibrations, the initial condition on the liquid surface displacements are set to -0.9 m in the first four columns and +0.9 m in the last four columns. The CFD simulations and analytical solutions of the liquid surface displacements match very well for the first 2 seconds. After that, as the system energy diminishes, the error slightly increases, but the analytical model can still capture the oscillation amplitude. In the forced vibration case, the TLMCD is subjected to a harmonic base acceleration $\ddot{x}_g = 0.6\sin(0.934t)$ m/s^2, where the vibration frequency is close to the first frequency of free vibration of the 8-column TLMCD, and the acceleration amplitude is selected arbitrarily to provide a reasonable fluid motion. The liquid motion is shown in Fig. 5. Results show a good agreement between the model and simulation results. It can also be observed that the liquid motion is almost at the same phase in all columns, with a slight decrease in phase from the left-most to the right-most column.

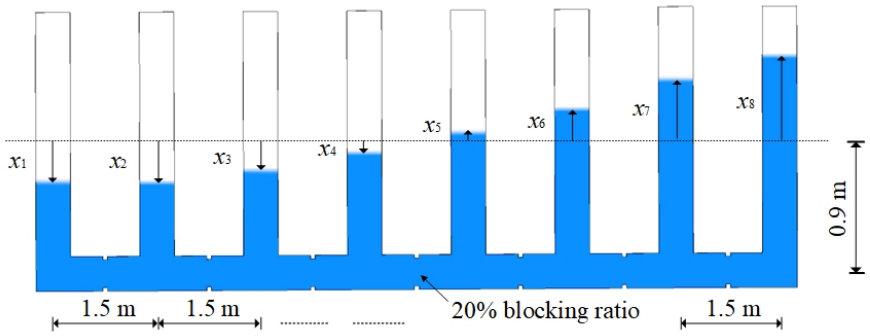

Figure 5: CFD results of the 8-column TLMCD under forced vibration, $t = 14.6$ s.

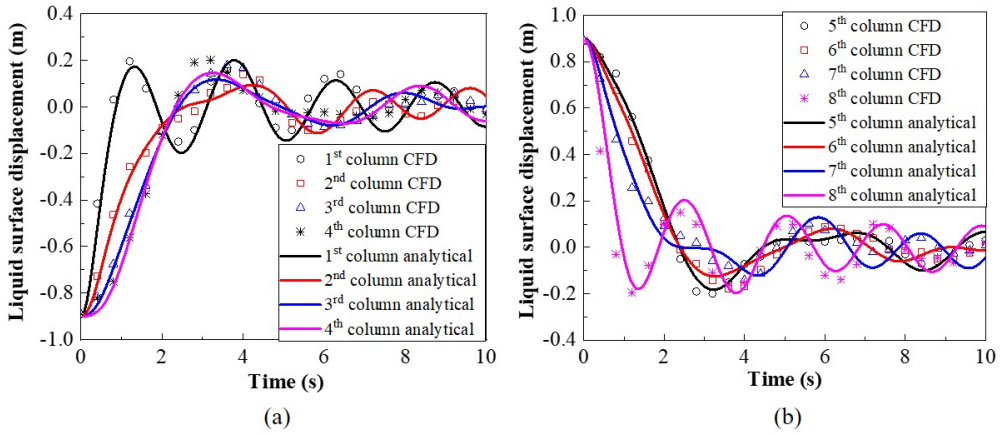

Figure 6: Time series of liquid displacements under free oscillation: (a) columns x_1 to x_4; and (b) columns x_5 to x_8.

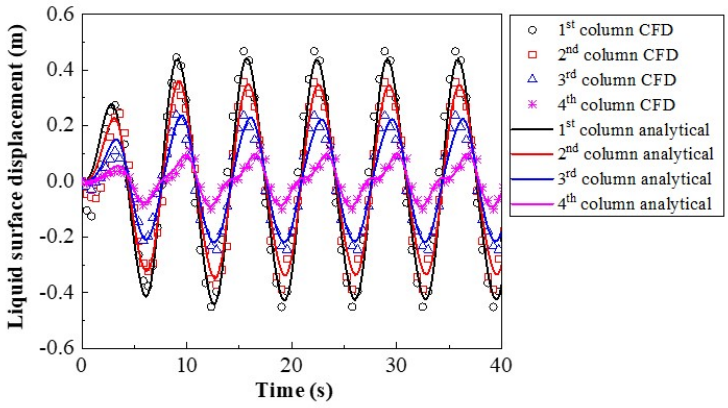

(a)

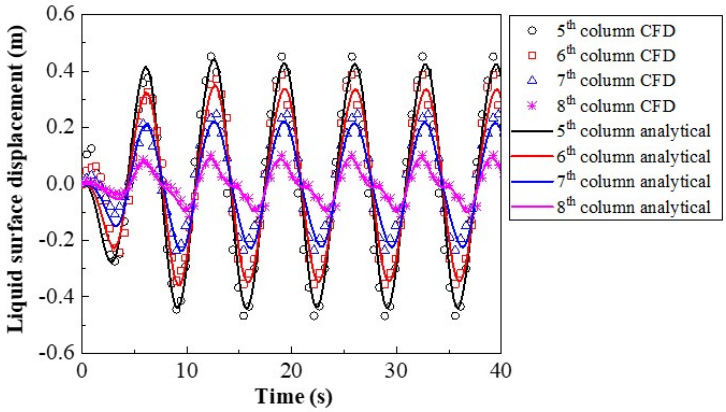

(b)

Figure 7: Time series of liquid displacements under free oscillation: (a) columns x_1 to x_4; and (b) columns x_5 to x_8.

4. Modal analysis

4.1. Weak nonlinearity of TLMCD

The nonlinear equations of motion in the TLMCD model makes it difficult to extract frequencies of free vibration analytically. For an undamped free vibration case, it is possible to calculate the system's frequencies of free vibration using invariant points, where these frequencies are solely determined by the system's energy regardless of initial conditions [23]. However, this method is not applicable to damped models and those under forced vibrations, because the system's energy is time-varying and invariant points are not available.

The weakly dependence of a nonlinear system's frequencies of free vibration can be measured by the fluctuation range of frequencies, and a small variation range indicates that frequencies are consistent under various situations. Mechanical systems with weak nonlinearity, in which the nonlinear terms in the differential equations of motion are much smaller than the linear ones, tend to have weakly dependent frequency response functions [34]. Various numerical simulations suggest that a TLMCD is a weakly nonlinear system, and that

frequencies of free vibration of TLMCDs can be identified numerically through resonance frequency responses under a harmonic frequency sweep. For example, the vibration amplitudes of the displacements of the first two columns of 4-column TLMCD with an equal column spacing of 1 m and an initial liquid height of 1 m under harmonic vibrations are obtained using Eq. (12). Fig. 8 plots the frequency responses under various orifice blocking ratios ψ. It can be observed that increasing the orifice blocking ratios only reduces the corresponding resonance frequencies of the TLMCD by less than 1%, as illustrated in Fig. 10(a). Another factor that may influence frequencies of free vibration is the total energy of the system, because a TLMCD's frequencies of free vibration may be input amplitude-dependent given its nonlinearity. Fig. 9 plots the frequency responses under harmonic excitation inputs with various amplitudes. It is found that increasing the acceleration input affects the frequency response amplitude almost proportionally, and that there is a small, insignificant drift in the resonance frequencies, as illustrated in Fig. 10(b). It can be concluded that a TLMCD is weakly nonlinear and its frequencies of free vibration can be estimated within a reasonable range independently of damping and system energy. The next section discusses how these frequencies and corresponding mode shapes can be analytically computed.

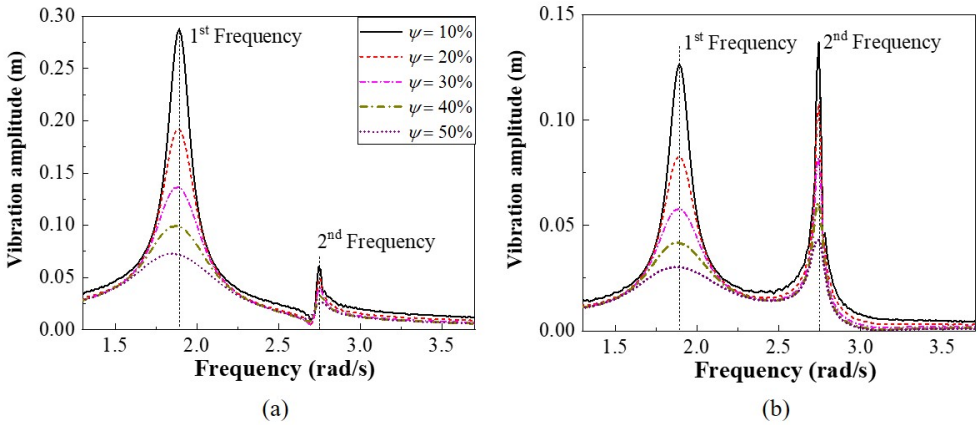

Figure 8: Frequency responses of a 4-column TLMCD under various uniform orifice blocking ratios (amplitude of $\ddot{x}_g = 0.1\text{m/s}^2$): (a) frequency response for x_1; and (b) frequency response for x_2.

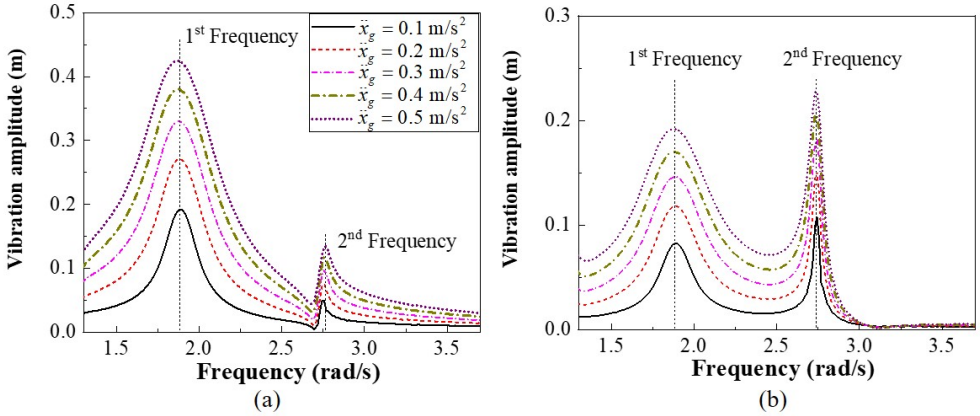

Figure 9: Frequency responses of a 4-column TLMCD under various acceleration amplitudes ($\psi = 20\%$): (a) frequency response for x_1; and (b) frequency response for x_2.

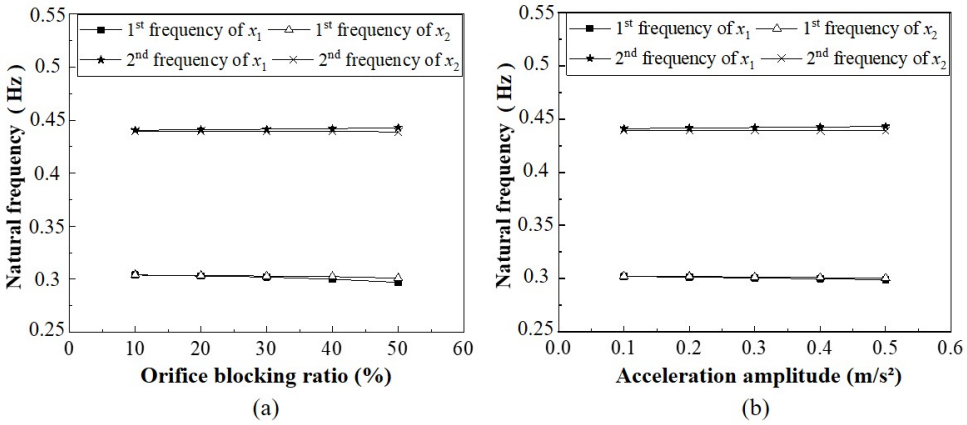

Figure 10: The influence of orifice damping and floor acceleration amplitudes on the 4-column TLMCD's frequency response: (a) orifice blocking ratio; and (b) acceleration amplitude.

4.2. Linearization method

Symmetric TLMCD

The nonlinearity of the TLMCD is attributed to the coupled liquid motion in multiple vertical columns. For a geometrically symmetric TLMCD, opposite columns have opposite liquid surface displacements. Based on this observation, the equations of motion for symmetrical TLMCDs can be linearized, and the rank of an N-column symmetrical TLMCD system can be reduced to $N/2$ (as frequencies of free vibration are equal

pairwise). The linearized constant mass and stiffness matrices are derived from Eq. (12):

$$\mathbf{M}=\begin{bmatrix} \nu\left(2\sum_{k=1}^{N/2}l_k-l_{N/2}\right)+2h & \nu\left(2\sum_{k=2}^{N/2}l_k-l_{N/2}\right) & \nu\left(2\sum_{k=3}^{N/2}l_k-l_{N/2}\right) & \dots & \nu l_{N-1} \\ \nu\left(2\sum_{k=2}^{N/2}l_k-l_{N/2}\right) & \nu\left(2\sum_{k=2}^{N/2}l_k-l_{N/2}\right)+2h & \nu\left(2\sum_{k=3}^{N/2}l_k-l_{N/2}\right) & \dots & \nu l_{N-1} \\ \nu\left(2\sum_{k=3}^{N/2}l_k-l_{N/2}\right) & \nu\left(2\sum_{k=3}^{N/2}l_k-l_{N/2}\right) & \nu\left(2\sum_{k=3}^{N/2}l_k-l_{N/2}\right)+2h & \dots & \nu l_{N-1} \\ \vdots & \vdots & \vdots & \ddots & \vdots \\ \nu l_{N-1} & \nu l_{N-1} & \nu l_{N-1} & \dots & \nu l_{N-1}+2h \end{bmatrix}_{N/2\times N/2} \tag{15}$$

$$\mathbf{K}=\begin{bmatrix} 2g & 0 & \dots & 0 \\ 0 & 2g & \dots & 0 \\ \vdots & \vdots & \ddots & \vdots \\ 0 & 0 & \dots & 2g \end{bmatrix}_{N/2\times N/2} \tag{16}$$

The frequencies of free vibration and mode shapes can be obtained directly from the linearized mass and stiffness matrices.

Another simple method can be also used to determine the frequencies of free vibration of the symmetric TLMCD. To better describe this method, the first mode shape of a TLMCD is shown in Fig. 11. The fundamental frequency of free vibration and mode shape of a TLMCD can be expressed physically using the frequency of free vibration formula of liquid column vibration absorbers (LCVAs). An LCVA is a variant of a TLCD where the cross-section area of the horizontal column is smaller than that of vertical columns [35]. A TLMCD's motion can be simplified as a combination of several independent LCVAs with the same frequency of free vibration. The effective length of a LCVA is given as [35]:

$$l_e=\nu l+2h \tag{17}$$

where l and h are the horizontal and vertical lengths of a LCVA, respectively. If an N-column symmetrical TLMCD is separated into $N/2$ individual LCVAs, their common frequency of free vibration can be calculated using the following equations:

$$\sum_{j=1}^{N/2}\alpha_j=1 \tag{18}$$

$$2h+\nu\left[\left(\sum_{i=j+1}^{N/2-1}2l_i\right)+l_{N/2}\right]/\alpha_j+2\nu l_j/\left(\sum_{i=1}^{j}\alpha_j\right)=l_e,\qquad j=1,2,...,N/2 \tag{19}$$

$$\omega=\sqrt{\frac{2g}{l_e}} \tag{20}$$

where α_j is the j^{th} cross-section area proportion in the horizontal middle column, l_e is the effective length of all LCVAs, and ω is the fundamental frequency of free vibration of the TLMCD. Solving the above equations for the fundamental frequency is straightforward if negative α_j values are always discarded. It is verified

that the result obtained from above equations is the same as that solved using the matrix form. In higher order vibration modes, α_j values can be negative and the calculation process is more complex.

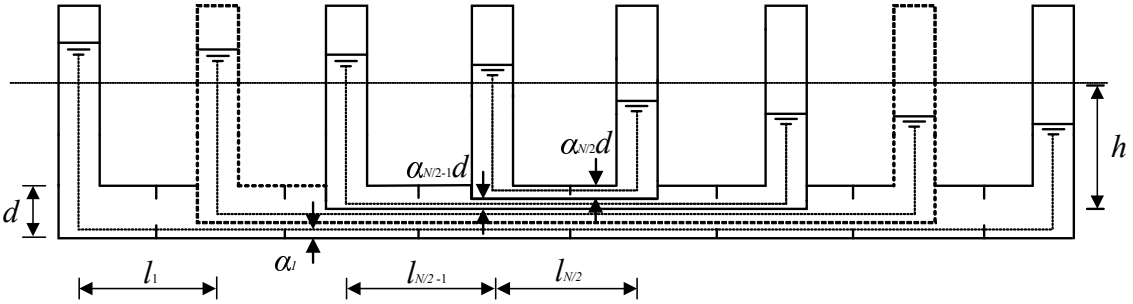

Figure 11: Fundamental vibration mode for a symmetric TLMCD.

Asymmetric TLMCDs

Asymmetric TLMCDs have stronger nonlinearities, and the frequencies of free vibration can only be obtained using an approximate method. If we neglect the nonlinear terms and the displacements in the Eq.(12), constant mass and stiffness matrices are derived:

$$\mathbf{M} = \begin{bmatrix} \nu\sum_{k=1}^{N-1} l_k + 2h & \nu\sum_{k=2}^{N-1} l_k + h & \nu\sum_{k=3}^{N-1} l_k + h & \dots & \nu l_{N-1} + h \\ \nu\sum_{k=2}^{N-1} l_k + h & \nu\sum_{k=2}^{N-1} l_k + 2h & \nu\sum_{k=3}^{N-1} l_k + h & \dots & \nu l_{N-1} + h \\ \nu\sum_{k=3}^{N-1} l_k + h & \nu\sum_{k=3}^{N-1} l_k + h & \nu\sum_{k=3}^{N-1} l_k + 2h & \dots & \nu l_{N-1} + h \\ \vdots & \vdots & \vdots & \ddots & \vdots \\ \nu l_{N-1} + h & \nu l_{N-1} + h & \nu l_{N-1} + h & \dots & \nu l_{N-1} + 2h \end{bmatrix}_{N-1\times N-1} \tag{21}$$

$$\mathbf{K} = \begin{bmatrix} 2g & g & \dots & g \\ g & 2g & \dots & g \\ \vdots & \vdots & \ddots & \vdots \\ g & g & \dots & 2g \end{bmatrix}_{N-1\times N-1} \tag{22}$$

It can be found that the mass and stiffness matrices from the asymmetric TLMCD (Eq. (21) and Eq. (22)) have different sizes and off-diagonal terms comparing with the linearized mass and stiffness matrices under the symmetric case (Eqs. (15) and (16)). In this situation, there are a total of N-1 frequencies of free vibration for an asymmetric N-column TLMCD. The frequencies of free vibration and mode shapes of the asymmetric TLMCD are calculated using Eqs. (21) and (22). Note that this method applies for small liquid displacements, and it should be used to approximately predict the frequencies of free vibration, but not the actual liquid motion.

4.3. Numerical Examples

The method for extracting frequencies of free vibration and mode shapes in Section 4.2 is illustrated using the 4-column and the 8-column TLMCD examples described in Section 3.2.

4-column TLMCD

The linearized mass and stiffness matrices for the symmetric 4-column TLMCD are obtained using Eqs. (15) and (16):

$$\mathbf{M} = \begin{bmatrix} \nu\left(2l_1 + l_2\right) + 2h & \nu l_2 \\ \nu l_2 & \nu l_2 + 2h \end{bmatrix} \tag{23}$$

$$\mathbf{K} = \begin{bmatrix} 2g & 0 \\ 0 & 2g \end{bmatrix} \tag{24}$$

The resulting mode shapes are:

$$\begin{bmatrix} \phi_1 & \phi_2 \end{bmatrix} = \begin{bmatrix} -0.924 & -0.383 \\ -0.383 & 0.924 \end{bmatrix} \tag{25}$$

From this linearization method, the 4-column TLMCD is separated into two smaller LCVAs that share the same frequency of free vibration. The cross-sectional area proportional to these two smaller horizontal columns, α_1 and α_2, can be obtained by equalizing the effective lengths of the two LCVAs (Eq. (19)). Two different sets of α_1 and α_2 values will be produced, corresponding to two frequencies of free vibration of the 4-column TLMCD. Fig. 12 shows the liquid flow inside the 4-column TLMCD when the damper is excited by a sinusoidal acceleration at its first and second frequencies of free vibration, respectively. It is observed that α_2 is negative in the second frequency response shape, where the flow direction in the middle horizontal column is reversed and contrary to the fluid flow's direction in the larger LCVA.

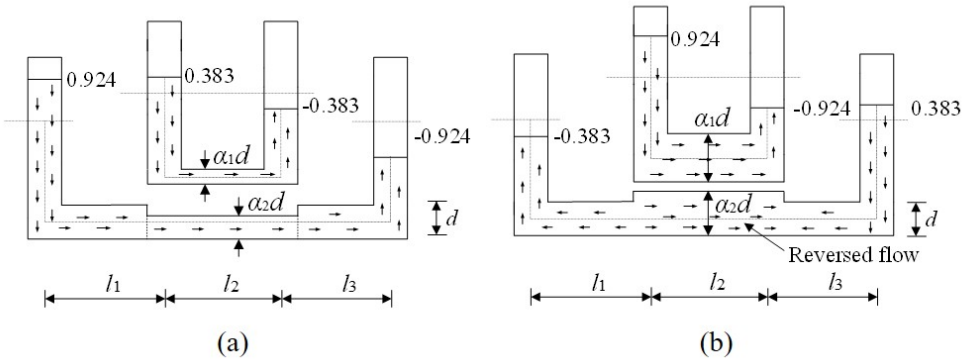

Figure 12: The 4-column TLMCD's response shapes: (a) the first frequency response shape; and (b) the second frequency response shape.

Table 3: Comparison of numerical (num) and analytical (analyt) frequencies of free vibration for TLMCDs with different column spacings.

case	type	column spacing (m)				1^{st} freq. (rad/s)		2^{nd} freq. (rad/s)		3^{rd} freq. (rad/s)		4^{th} freq. (rad/s)	
		l_1	l_2	l_3	l_4	num	analyt	num	analyt	num	analyt	num	analyt
1	symmetric 4-column TLMCD	1	0.5	1	–	2.37	2.33	3.76	3.77	–	–	–	–
2		1	1	1	–	2.09	2.11	3.52	3.48	–	–	–	–
3		1	2.5	1	–	1.67	1.65	3.27	3.30	–	–	–	–
4		1	5	1	–	1.27	1.27	3.20	3.21	–	–	–	–
5	asymmetric 4-column TLMCD	0.5	0.5	1	–	2.46	2.47	3.41	3.46	3.88	3.87	–	–
6		1	2	3	–	1.53	1.55	2.57	2.62	3.19	3.20	–	–
7	symmetric 8-column TLMCD	0.9	0.9	0.9	0.9	1.12	1.15	2.06	2.10	2.31	2.31	2.38	2.38

To validate the robustness and accuracy of the frequency of free vibration analytical computation method, various column spacings in the 4-column TLMCD are studied, as shown in Table 3. The frequencies results calculated from the analytical method are compared with numerical results which are simulated using the numerical methods described in Section 4.1. The comparison between the identified analytical and numerical frequencies show a good agreement, as all the differences are less than 2%. Frequency response curves of the simulated first column liquid surface displacement x_1 under Cases 2 and 5 are plotted in Fig. 13. It is found that there are two distinctive frequencies of free vibration for the symmetric case (Case 2 in Table 3) and three for the asymmetric case (Case 5 in Table 3).

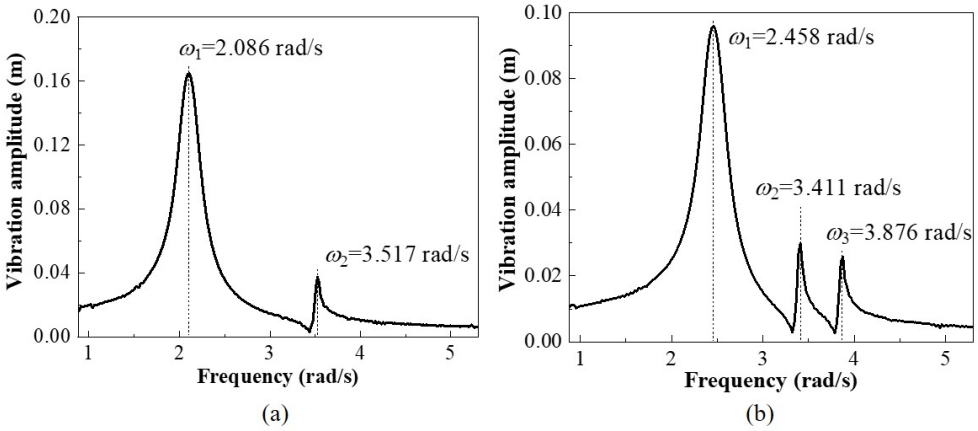

Figure 13: Frequency response curves of x_1 for 4-column TLMCDs: (a) a symmetric case (Case 2 in Table 3); and (b) an asymmetric case (Case 5 in Table 3).

8-column TLMCD

The equally spaced (symmetric) 8-column TLMCD is also simulated (Case 7) and results in Table 3 show good agreement between the analytical and numerical frequencies. Fig. 14 plots the frequency response of the first column liquid surface displacement x_1. The first analytical mode shape, as illustrated in Fig. 15, also correlates to that of the CFD simulation (see Fig. 5). Higher order mode shapes can be described by

the corresponding mode shape coefficients. Given the same total horizontal length, increasing the column number will significantly lower all the frequencies of free vibration. If required, this can be compensated, for example, by enlarging the horizontal tube's cross-section. The next section presents a parametric study to further the understanding of TLMCD alterations.

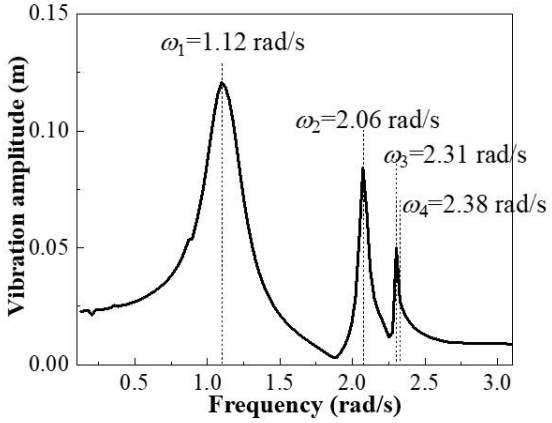

Figure 14: Frequency response of x_1 for the 8-column TLMCD (amplitude of $\ddot{x}_g = 0.1$ m/s^2, $\psi = 20$ %).

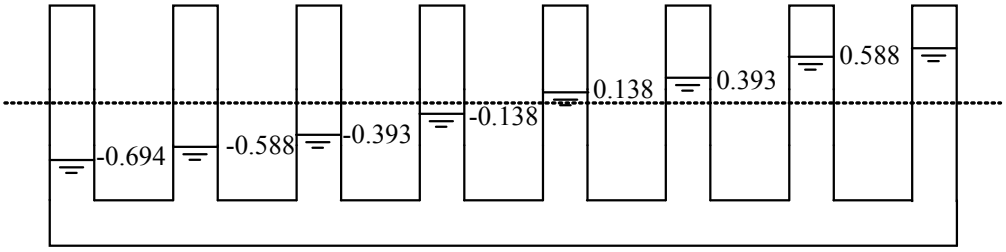

Figure 15: Fundamental mode shape of the 8-column TLMCD.

5. Parametric study of damping performance for an SDOF structure

The damping performance of a TLCD or a TLMCD is usually measured by its capability to reduce structural responses [36]. In this section, the transfer function H_1, defined as the ratio of the dynamic displacement amplitude to the static structural response (Eq. (26)), is used to evaluate the TLMCD's damping capacity, whereas the main mitigation objective is to lower the maximum H1 value across all frequencies

$$H_1 = \frac{|x_s|_{\max}}{p_0/k_s} \tag{26}$$

where x_s is the SDOF structure's displacement, p_0 is the base harmonic excitation amplitude, and k_s is the structural stiffness. We apply harmonic ground motions to the TLMCD-structure system and evaluate the parametric effects, including tuning ratios, head loss coefficients, and column configurations, on H_1.

In literature on TLCDs, analytical transfer functions for structural responses are only available after the nonlinear damping force due to the head loss is linearized. Because the system of interest is nonlinear, H_1 is numerically evaluated using the steady state of the structural response. The equation of motion governing the SDOF system equipped with a TLMCD is written as

$$m_s\ddot{x}_s + \rho_l A\left(Nh + \sum_{i=1}^{N-1} l_i/\nu\right)\ddot{x}_s + \rho_l A\sum_{i=1}^{N-1}\left(\ddot{x}_i\sum_{j=1}^{i} l_j\right) + c_s\dot{x}_s + k_s x_s = p_0\sin(\omega_f t) \tag{27}$$

where c_s is the structural damping coefficient, ω_f is the excitation frequency. The SDOF system equipped with the TLMCD is numerically simulated using Eqs. (12) and (27) to estimate H_1.

In the following parametric studies, the configuration of the TLMCD, illustrated in Fig. 16, is as follows. The mass ratio γ is 1%, and the initial liquid heights in the vertical columns are set to a uniform value $h = 0.853$ m. The structural characteristics of the SDOF structure are taken as $m_s = 386100$ kg, $\omega_s = 1.1$ rad/s, and $\xi_s = 0.05$. A harmonic force with an amplitude of $p_0 = 0.001 m_s g$ and with frequencies ranging from 80% to 120% of the TLMCD's first frequency of free vibration, which can be identified using the method described in Section 4, is applied to the structure. The effect of column spacing l_i, cross-section area ratio ν, orifice head loss coefficient η, and column number N on the structural vibration responses are investigated.

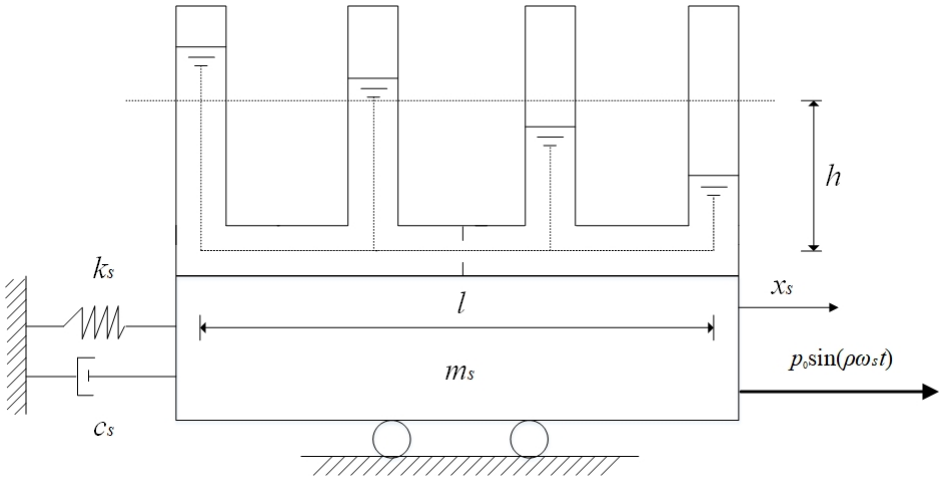

Figure 16: SDOF system equipped with a TLMCD.

5.1. Tuning frequency ratios

The TLMCD's tuning frequency ratio χ is defined as the ratio of the damper's first frequency of free vibration to the structure's natural frequency. There are two parameters that can be used to tune the TLMCD's first frequency of free vibration: the cross-section area ratio ν and the column spacing l_i.

To study the effect of column spacing, we set parameters ν, η and h constant and vary l_i. The relationship between l_i and ν and χ is estimated using the linearization method in Section 4.2 and plotted in Fig. 17 (a), showing that as l_i increases χ decreases. The task is repeated for ν, with the behavior plotted in Fig. 17 (b), exhibiting χ decreasing for ν increasing.

The effect of the parameters on H_1 is investigated on a 4-column and an 8-column TLCD, whose properties are listed in Table 4. Fig. 18 plots H_1 versus ρ curves for various values of l_i, and Fig. 19 plots H_1 versus ρ curves for various values of ν. Results show that there exists an optimal tuning ratio that can be obtained through tuning either or both parameters. This optimal value is characterized by two peaks of equal height.

It can be noted that the 4-column TLMCD is more sensitive to variations in l_i and ν than the 8-column one, and that the 8-column TLMCD is less effective around resonance.

Table 4: TLMCDs parameters for study of different tuning frequency ratios.

parameters		units	4-column	8-column
liquid height	h	m	0.853	0.853
mass ratio	γ	%	1.0	1.0
orifice head loss coefficient	η	–	1.5	0.4
column spacing	l_i	m	(5.118)	(2.193)
cross-section area ratio	ν	–	(1.017)	(0.615)

Note: The values in parentheses are those used when kept constant.

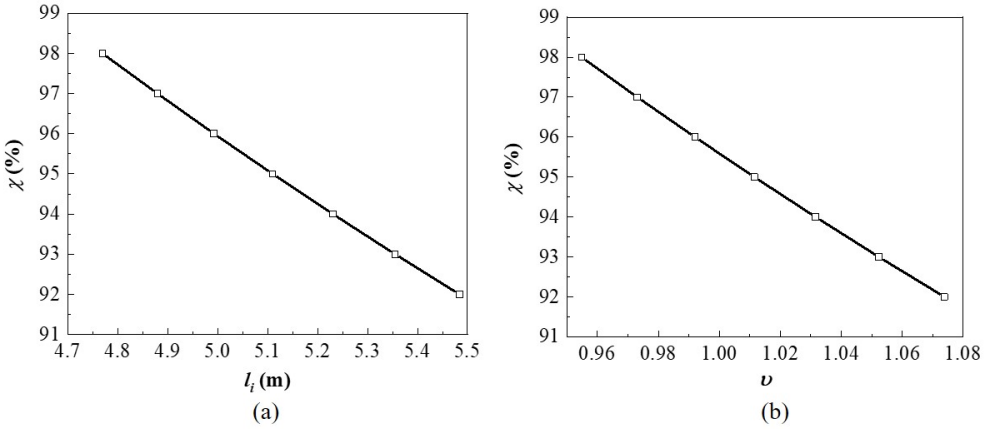

Figure 17: Effect of (a) column spacing l_i; and (b) cross-section area ratio υ on the tuning ratio.

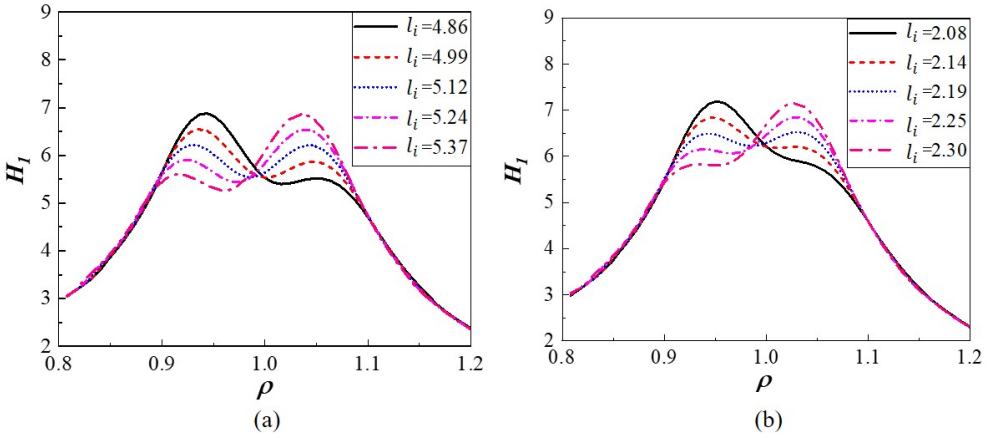

Figure 18: Effect of column spacing l_i for: (a) 4-column TLMCD; and (b) 8-column TLMCD.

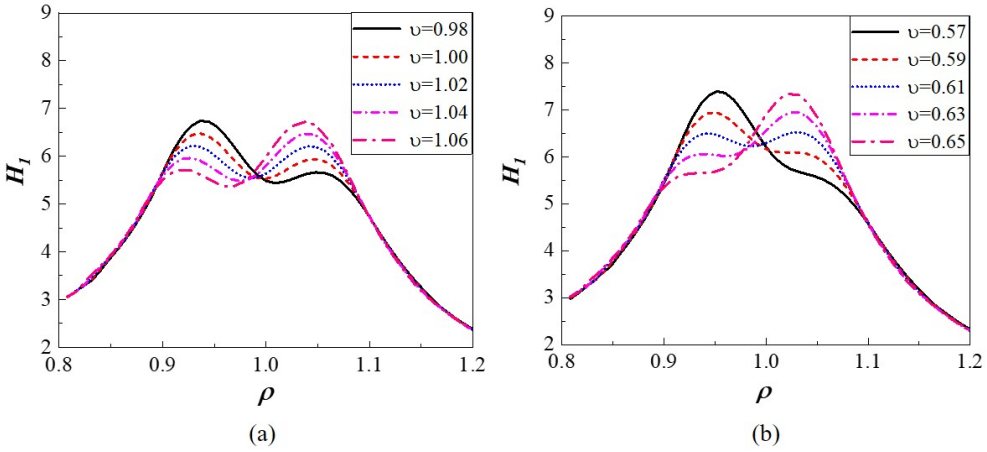

Figure 19: Effect of cross-section area ratio υ for: (a) 4-column TLMCD; and (b) 8-column TLMCD.

5.2. Head loss coefficients

Here, values for l_i and ν are fixed, taken at the optimal tuning ratios found in the previous section. Simulation parameters for the 4-column and 8-column TLMCDs are listed in Table 5. The head loss coefficient for each orifice is taken as identical and altered simultaneously. Their effects on H_1 are plotted in Fig. 20. Two invariant points can be observed in the transfer functions that are independent of the head loss coefficients. It follows that the optimized head loss coefficients are those that result in the invariant points being the highest in H_1. It can also be noted that, because it has fewer orifices, the 4-column TLMCD requires larger head loss coefficients ($\eta = 2$) to minimize H_1 than does the 8-column TLMCD ($\eta = 0.5$).

Table 5: TLMCDs parameters for study of different head loss coefficients.

parameters		units	4-column	8-column
total length	l	m	17.059	17.059
liquid height	h	m	0.853	0.853
mass ratio	γ	%	1.0	1.0
column spacing	l_i	m	5.118	2.193
cross-section area ratio	ν	–	1.017	0.615

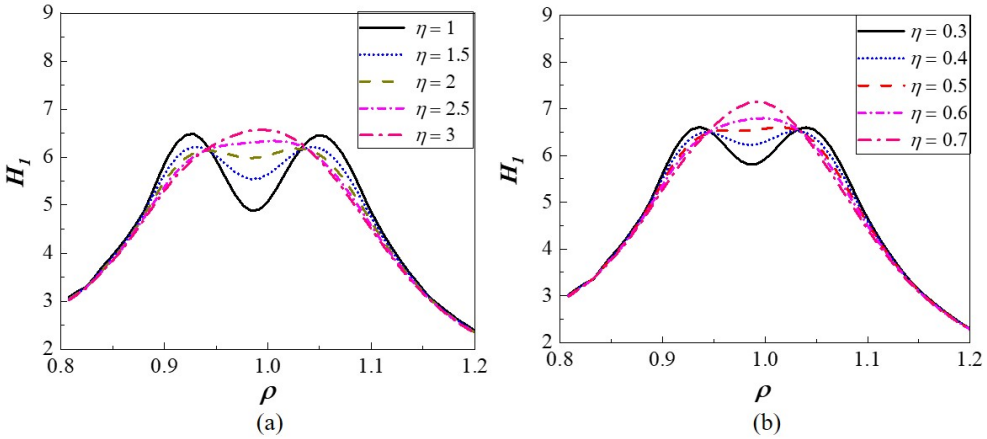

Figure 20: Effect of orifice head loss coefficient η for: (a) 4-column TLMCD; and (b) 8-column TLMCD.

5.3. Number of columns

The effect of the number of columns on the TLMCDs of parameters listed in Tables 6 and 7 are compared against each other. The minimized H_1 under various column numbers are plotted in Fig. 21(a) for an equal mass and in Fig. 21(b) for an equal column size throughout the studied configurations. The minimized H_1 were obtained by adjusting ν to obtain two equal peaks in the transfer function, and then adjusting the head loss coefficients to minimize the height of the peaks.

Results show that, when the total mass of the TLMCD is maintained constant, reducing the number of columns provides a better mitigation performance around resonance, but a slightly worse one in other frequency ranges. This is attributed to more mass of liquid present in the horizontal column, making the device more effective [12]. For a constant mass, a TLMCD will not over-perform a TLCD (2-column TLMCD). Conversely, when the mass ratio is allowed to vary but the size of the columns is maintained constant (Fig. 21(b)), increasing the number of columns provides better mitigation. This can be attributed to the larger mass ratio. In this case, a TLMCD could be designed to over-perform a TLCD. Overall, it can be concluded from results that, given a space constraint, a TLMCD could provide higher mitigation benefits compared with a TLCD. Remark that, not shown, it was observed that increasing the number of columns beyond 12 only had a non-significant effect to the overall response.

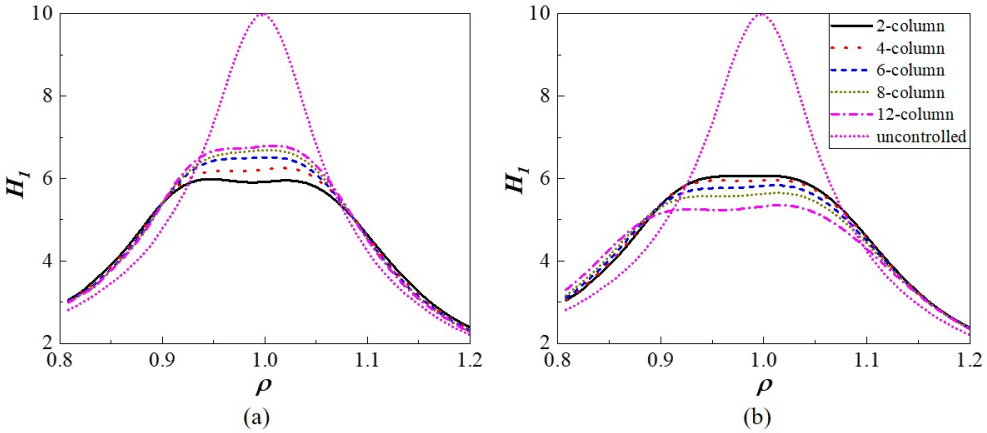

Figure 21: Comparison of the minimized transfer function curves under different column number N: (a) for equal mass; (b) for equal column size.

Table 6: Parameters for TLMCDs with different column number under equal liquid mass.

parameters		units	column number				
			2	4	6	8	12
total length	l	m	17.059	17.059	17.059	17.059	17.059
liquid height	h	m	0.853	0.853	0.853	0.853	0.853
mass ratio	γ	%	1.0	1.0	1.0	1.0	1.0
orifice head loss coefficient	η	–	10.2	2.3	1.0	0.5	0.22
vertical column size	A	m^2	0.295	0.237	0.175	0.137	0.099
cross-section area ratio	ν	–	1.152	1.017	0.772	0.615	0.432

Table 7: Parameters for TLMCDs with different number of columns of equal vertical heights.

parameters		units	column number				
			2	4	6	8	12
total length	l	m	17.059	17.059	17.059	17.059	17.059
liquid height	h	m	0.853	0.853	0.853	0.853	0.853
mass ratio	γ	%	1.0	1.5	2.0	2.6	3.7
orifice head loss coefficient	η	–	10.2	3.0	1.7	1.2	0.7
vertical column size	A	m^2	0.295	0.295	0.295	0.295	0.295
cross-section area ratio	ν	–	1.152	1.019	0.786	0.631	0.452

5.4. Structural mitigation using higher order modes of TLMCDs

The parameters of TLMCDs using the second vibration mode for structure mitigation are listed in Table 8. Higher order vibration modes of TLMCDs usually have smaller effective masses, and as a result, their damping ability is lower than the TLMCD's first vibration mode. Tuning higher order frequencies of free vibration to the natural frequency of the structure also requires significantly increasing the ν value, resulting in reduction of the percentage of liquid mass in the horizontal column and deterioration of TLMCDs' damping capability. The H_1 curves of 4-column and 8-column TLMCDs with different cross-section ratios are shown in Fig. 22, where $\nu = 5.7$ and $\nu = 4.9$ correspond to the optimized cases, respectively. Comparing against cases using the first vibration mode (Fig. 19), the structure yields a larger displacement response. Note that the distances between higher order frequencies are much closer to each other than the first two frequencies, and the transfer functions curves are possibly influenced by multiple vibration modes.

Table 8: TLMCDs parameters using the second vibration mode for structural mitigation.

parameters		units	4-column	8-column
total length	l	m	17.059	17.059
liquid height	h	m	0.853	0.853
mass ratio	γ	%	1.0	1.0
column spacing	l_i	m	5.118	2.193
uniform head loss coefficient	ν	–	1.017	0.615

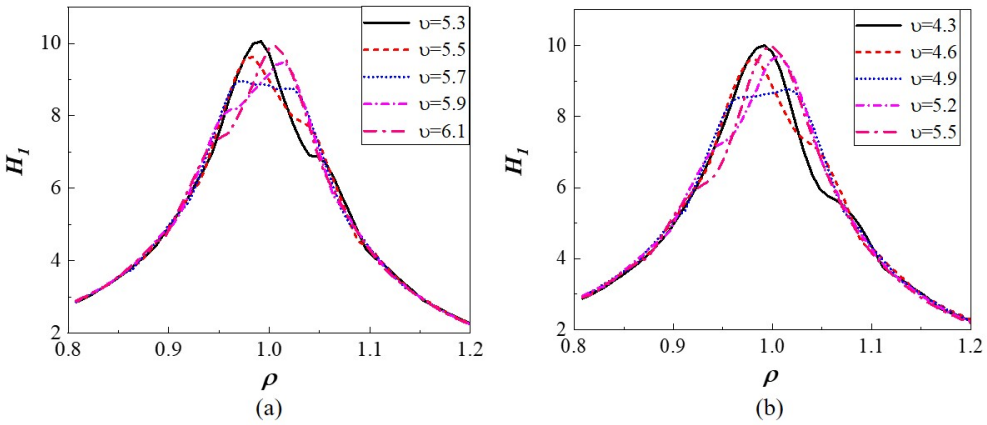

Figure 22: Transfer function curves using the second vibration mode for structural mitigation: (a) 4-column TLMCD; and (b) 8-column TLMCD.

6. Conclusions

In this paper, a nonlinear dynamic model for TLMCDs is derived using Lagrange equations to characterize both nonlinear orifice and friction damping forces. Both the analytical model and CFD method are used

to study two typical TLMCDs. Good correlations of liquid motion between both sets of results under both free oscillation and forced vibrations demonstrate the accuracy of the derived analytical model. Numerical simulation shows that the analytical model of the TLMCD is weakly nonlinear, and the influence of damping and system energy on the frequencies of free vibration of the TLMCD is limited. A simplified linearization method is developed to calculate the frequencies of free vibration of the TLMCD, which is validated by the numerical results of frequency response curves. The shape of the fundamental mode of TLMCD can be physically explained using the concept of the effective length from LCVAs.

A parametric study using the analytical model is conducted to evaluate the influence of various parameters on the reduction of structural vibration responses under harmonic excitations. It is found that the tuning ratio affects the shape of transfer function curve and can be adjusted to equalize the curve's two peaks by varying the column spacing or cross-section area ratio. Head loss coefficients control the damping force in TLMCD, which can be optimized for a fixed TLMCD configuration to minimize the structural response at resonance. The number of columns determines the portion of horizontal liquid mass in the TLMCD and indirectly influences the peak values of the transfer function curve.

It can be concluded that a two-column TLCD can be treated as a special type of TLMCD with the smallest number of columns. With the same mass ratio and liquid height, a TLMCD with more vertical columns is less effective than a TLCD, because the TLMCD has smaller horizontal mass. However, when keeping the geometries constant, a TLMCD with more columns over-performs a TLCD, because the TLMCD has a larger mass ratio.

This study focused on structural mitigation using the first vibration mode of TLMCDs. Although higher order vibration modes have less effective mass and may not be as effective as the first mode, it is still possible to combine a TLMCD's multiple vibration modes to mitigate structural responses, which is left to future work.

7. Acknowledgements

This material is based upon the work supported by the National Science Foundation under Grant No. CMMI-1562992. Any opinions, findings, and conclusions or recommendations expressed in this material are those of the authors and do not necessarily reflect the views of the National Science Foundation.

References

[1] A. Nespoli, D. Rigamonti, M. Riva, E. Villa, F. Passaretti, Study of pseudoelastic systems for the design of complex passive dampers: static analysis and modeling, Smart Mater Struct 25 (2016) 105001.

[2] S. De, S. F. Wojtkiewicz, E. A. Johnson, Efficient optimal design and design-under-uncertainty of passive control devices with application to a cable-stayed bridge, Struct Control Health Monit 24 (2017) e1846.

[3] Y. Gong, L. Cao, S. Laflamme, S. Quiel, J. Ricles, D. Taylor, Characterization of a novel variable friction connection for semiactive cladding system, Struct Control Health Monit 25 (2018) e2157.

[4] A. Downey, L. Cao, S. Laflamme, D. Taylor, J. Ricles, High capacity variable friction damper based on band brake technology, Eng Struct 113 (2016) 287–298.

[5] L. Cao, A. Downey, S. Laflamme, D. Taylor, J. Ricles, Variable friction device for structural control based on duo-servo vehicle brake: Modeling and experimental validation, J Sound Vib 348 (2015) 41–56.

[6] F. Ubertini, Active feedback control for cable vibrations, Smart Struct Syst 4 (2008) 407–428.

[7] A. V. Lysenko, N. Goryachev, N. K. Yurkov, A. Telegin, V. A. Trusov, Information-measuring control system of active vibration protection red, 2016 IEEE East-West Design & Test Symposium (EWDTS) (2016) 1–4.

[8] M. Symans, F. Charney, A. Whittaker, M. Constantinou, C. Kircher, M. Johnson, R. McNamara, Energy dissipation systems for seismic applications: current practice and recent developments, J Struct Eng 134 (2008) 3–21.

[9] J. Connor, S. Laflamme, Structural motion engineering, volume 483, Springer, (2014).

[10] B. Spencer Jr, S. Nagarajaiah, State of the art of structural control, J Struct Eng 129 (2003) 845–856.

[11] F. Sakai, Tuned liquid column damper-new type device for suppression of building vibration, Proceedings of International Conference on High-rise Buildings, (1989), pp. 926–931.

[12] H. Gao, K. Kwok, B. Samali, Optimization of tuned liquid column dampers, Eng Struct 19 (1997) 476–486.

[13] K.-W. Min, H.-S. Kim, S.-H. Lee, H. Kim, S. K. Ahn, Performance evaluation of tuned liquid column dampers for response control of a 76-story benchmark building, Eng Struct 27 (2005) 1101–1112.

[14] S. K. Yalla, A. Kareem, Optimum absorber parameters for tuned liquid column dampers, J Struct Eng 126 (2000) 906–915.

[15] K. Shum, Closed form optimal solution of a tuned liquid column damper for suppressing harmonic vibration of structures, Eng Struct 31 (2009) 84–92.

[16] M. Hochrainer, Tuned liquid column damper for structural control, Acta Mechanica 175 (2005) 57–76.

[17] P. Hitchcock, K. Kwok, R. Watkins, B. Samali, Characteristics of liquid column vibration absorbers (LCVA)I, Eng Struct 19 (1997) 126–134.

[18] L. Rozas, R. L. Boroschek, A. Tamburrino, M. Rojas, A bidirectional tuned liquid column damper for reducing the seismic response of buildings, Struct Control Health Monit 23 (2016) 621–640.

[19] K.-W. Min, C.-S. Park, J. Kim, Easy-to-tune reconfigurable liquid column vibration absorbers with multiple cells, Smart Mater Struct 24 (2015) 065041.

[20] H. Wu, L. Cao, A. Chen, S. Laflamme, A novel tuned liquid wall damper for multi-hazard mitigation, in: Active and Passive Smart Structures and Integrated Systems, volume 10164, International Society for Optics and Photonics, (2017), p. 1016433.

[21] F. Ubertini, G. Comanducci, S. Laflamme, A parametric study on reliability-based tuned-mass damper design against bridge flutter, J Vib Control 23 (2017) 1518–1534.

[22] H. Gao, K. Kwok, B. Samali, Characteristics of multiple tuned liquid column dampers in suppressing structural vibration, Eng Struct 21 (1999) 316–331.

[23] K. Hirata, A. D. Craik, Nonlinear oscillations in three-armed tubes, European Journal of Mechanics-B/Fluids 22 (2003) 3–26.

[24] P. Hitchcock, K. Kwok, R. Watkins, B. Samali, The effectiveness of a multiple liquid column vibration absorber, in: Proceedings of the 4th Workshop on Wind Engineering, Australian Wind Engineering Society, (1994), pp. 81–86.

[25] A. Sarkar, O. T. Gudmestad, Pendulum type liquid column damper (plcd) for controlling vibrations of a structure–theoretical and experimental study, Eng Struct 49 (2013) 221–233.

[26] I. E. Idelchik, Handbook of hydraulic resistance, Washington, DC, Hemisphere Publishing Corp., 1986, 662 p. Translation. (1986).

[27] K.-W. Min, Y.-W. Kim, J. Kim, Analytical and experimental investigations on performance of tuned liquid column dampers with various orifices to wind-excited structural vibration, J Wind Eng Ind Aerod 139 (2015) 62–69.

[28] J.-C. Wu, M.-H. Shih, Y.-Y. Lin, Y.-C. Shen, Design guidelines for tuned liquid column damper for structures responding to wind, Eng Struct 27 (2005) 1893–1905.

[29] S. Colwell, B. Basu, Investigations on the performance of a liquid column damper (LCD) with different orifice diameter ratios, Canadian J of Civil Eng 33 (2006) 588–595.

[30] A. Di Matteo, F. Lo Iacono, G. Navarra, A. Pirrotta, Numerical and experimental validation of a simplified formulation for the design of tlcd, in: 11th international conference on structural safety & reliability, (2013), pp. 16–20.

[31] H. Shad, A. B. Adnan, H. P. Behbahani, Performance evaluation of tuned liquid dampers on response of a sdof system under earthquake excitation and harmonic load, Res J Appl Sci Eng Tech 6 (2013) 3018–3021.

[32] J. Sun, G. Y. Li, L. Liu, Q. B. Liu, The tlcd u-tube liquid sloshing finite element modal analysis, in: Adv Mat Res, volume 694, Trans Tech Publ, (2013), pp. 350–353.

[33] N. Cavalagli, C. Biscarini, A. L. Facci, F. Ubertini, S. Ubertini, Experimental and numerical analysis of energy dissipation in a sloshing absorber, J Fluids Struct 68 (2017) 466–481.

[34] A. F. Vakakis, D. Ewins, Effects of weak non-linearities on modal analysis, Mech Syst Signal Process 8 (1994) 175–198.

[35] R. Watkins, Tests on a liquid column vibration absorber for tall structures, Steel Structures: Recent Research and Developments, Singapore 22 (1991).

[36] L. Cao, S. Laflamme, D. Taylor, J. Ricles, Simulations of a variable friction device for multihazard mitigation, J Struct Eng 142 (2016) H4016001.

Table caption list

Table 1: Comparison of liquid surface amplitudes (cm) between CFD and test results [28].

Table 2: System parameters for 4-column and 8-column TLMCDs.

Table 3: Comparison of numerical (num) and analytical (analyt) frequencies of free vibration for TLMCDs with different column spacings.

Table 4: TLMCDs parameters for study of different tuning frequency ratios.

Table 5: TLMCDs parameters for study of different head loss coefficients.

Table 6: Parameters for TLMCDs with different column number under equal liquid mass.

Table 7: Parameters for TLMCDs with different number of columns of equal vertical heights.

Table 8: TLMCDs parameters using the second vibration mode for structural mitigation.

Figure caption list

Fig. 1: Schematic of an N-column TLMCD (x_i is positive upwards).

Fig. 2: Time series of column displacements under free oscillation: (a) columns x_1 and x_2; and (b) columns x_3 and x_4.

Fig. 3: CFD results of the 4-column TLMCD under forced vibration, $t = 7.8$ s.

Fig. 4: Time series of column displacements under forced oscillation: (a) columns x_1 and x_2; and (b) columns x_3 and x_4.

Fig. 5: CFD results of the 8-column TLMCD under forced vibration, $t = 14.6$ s.

Fig. 6: Time series of liquid displacements under free oscillation: (a) columns x_1 to x_4; and (b) columns x_5 to x_8.

Fig. 7: Time series of liquid displacements under free oscillation: (a) columns x_1 to x_4; and (b) columns x_5 to x_8.

Fig. 8: Frequency responses of a 4-column TLMCD under various uniform orifice blocking ratios (amplitude of $\ddot{x}_g = 0.1\text{m/s}^2$): (a) frequency response for x_1; and (b) frequency response for x_2.

Fig. 9: Frequency responses of a 4-column TLMCD under various acceleration amplitudes ($\psi = 20\%$): (a) frequency response for x_1; and (b) frequency response for x_2.

Fig. 10: The influence of orifice damping and floor acceleration amplitudes on the 4-column TLMCD's frequencies of free vibration: (a) orifice blocking ratio; and (b) acceleration amplitude.

Fig. 11: Fundamental vibration mode for a symmetric TLMCD.

Fig. 12: The 4-column TLMCD's response shapes: (a) the first frequency response shape; and (b) the second frequency response shape.

Fig. 13: Frequency response curves of x_1 for 4-column TLMCDs: (a) a symmetric case (Case 2 in Table 3); and (b) an asymmetric case (Case 5 in Table 3).

Fig. 14: Frequency response of x_1 for the 8-column TLMCD (amplitude of $\ddot{x}_g = 0.1$ m/s^2, $\psi = 20$ %).

Fig. 15: Fundamental mode shape of the 8-column TLMCD.

Fig. 16: SDOF system equipped with a TLMCD.

Fig. 17: Effect of (a) column spacing l_i; and (b) cross-section area ratio υ on the tuning ratio.

Fig. 18: Effect of column spacing l_i for: (a) 4-column TLMCD; and (b) 8-column TLMCD.

Fig. 19: Effect of cross-section area ratio υ for: (a) 4-column TLMCD; and (b) 8-column TLMCD.

Fig. 20: Effect of orifice head loss coefficient η for: (a) 4-column TLMCD; and (b) 8-column TLMCD.

Fig. 21: Comparison of the minimized transfer function curves under different column number N: (a) for equal mass; (b) for equal column size.

Fig. 22: Transfer function curves using the second vibration mode for structural mitigation: (a) 4-column TLMCD; and (b) 8-column TLMCD.